Received: 18 May 2018 | Revised: 19 August 2018 | Accepted: 25 August 2018

DOI: 10.1002/aoc.4606

WILEY Applied Organometallic Chemistry

FULL PAPER

Nano-synthesis, characterization, modeling and molecular docking analysis of Mn (II), Co (II), Cr (III) and Cu (II) complexes with azo pyrazolone ligand as new favorable antimicrobial and antitumor agents

Mohamed Gaber[1] | Abdalla M. Khedr[1,2] | Mohammed A. Mansour[3,4] | Mohsen Elsharkawy[1]

[1] Chemistry Department, Faculty of Science, Tanta University, Tanta 31527, Egypt

[2] Department of Chemistry, Faculty of Applied Science, Umm Al–Qura University, Makkah, Saudi Arabia

[3] Biochemistry Division, Chemistry Department, Faculty of Science, Tanta University, Tanta 31527, Egypt

[4] Institute of Cancer Sciences, University of Glasgow, Garscube Estate, Switchback Road, Glasgow G61 1QH, UK

Correspondence
Abdalla M. Khedr, Department of Chemistry, Faculty of Applied Science, Umm Al–Qura University, Makkah, Saudi Arabia.
Email: abkhedr2010@yahoo.com

Novel nanosized Mn (II), Co (II), Cr (III) and Cu (II) complexes were synthesized with 2-((5-oxo-1,3-diphenyl-4,5-dihydro-1H-pyrazol-4-yl)diazenyl) benzoic acid, HL applying precipitation method. Their structures were characterized based on the elemental and thermal analyses, spectra (FT-IR, UV–Vis, MS, ESR and XRD), conductivity and magnetic moment measurements. IR spectra offered that HL behaves as monobasic tri-dentate ligand towards Mn (II), Cr (III) and Cu (II) and monobasic bi-dentate towards Co (II). The XRD results unambiguously confirmed the crystalline nature and nano-sized particles of Cu (II) complex while HL and other complexes exhibited amorphous phases. The magnetic moment data, UV–Vis and ESR spectra supported the formation of octahedral geometries for Mn (II), and Cr (III) complexes, whereas Co (II), and Cu (II) complexes showed tetrahedral arrangement. The activation parameters for the thermal degradation stages were theoretically calculated using TGA curves. The obtained data showed the inspected complexes as favorable antimicrobial drug candidates. The studied compounds were screened out for their antitumor and antimicrobial activities. The inspected compounds exhibited a reasonable antibacterial activity and weak antitumor efficacy. The in vitro results were confirmed using the *in silico* molecular docking analysis (docking server) applying x-ray crystallographic structures of the proteins (4 m01, 3 t88, 1zap & 4ynt) from PDB (Protein Data Bank). HL and probably its complexes displayed adequate binding with the receptors of 4 m01, 3 t88, 1zap, and 4ynt microorganisms. The obtained data show the inspected complexes as favorable antimicrobial drug candidates.

KEYWORDS
antimicrobial, antitumor, modeling, molecular docking, nanosized metal complexes

1 | INTRODUCTION

Pyrazolones are defined as oxo five-membered heterocycle derivatives comprising two neighboring nitrogen atoms. They contain two double bonds inside the moiety; imparting an aromatic character to these molecules. Pyrazolones are still economically important precursors for both pharmaceuticals and dyes.[1] Pyrazolone derivatives have numerous pharmacological applications like analgesic,[2] antipyretic, anti-inflammatory,[3] antibacterial, antifungal,[4] anti-infective,[5] antioxidant,[6] anticonvulsant, anti-depressant, anti-hyperglycemic and anti-proliferative agents. Besides, they have the ability to extend noteworthy anticancer influences by inhibiting diverse types of enzymes that act serious roles in cell division.[7] 4-Aminoantipyrine is one of the superior celebrated pyrazolone derivatives which is applied for the protection towards oxidative stress and has a prophylactic influence on various diseases involving cancer.[8,9] Due to the reactivity of position-4 in the pyrazolone ring, it undergoes a coupling reaction with a number of aryl diazonium chlorides forming 4-arylazo derivatives, which are considered as an important class of azo dyes. The azo-derivatives of pyrazolone compounds have enticed great interest because of their prospect prominence in medicinal chemistry as antimicrobial agents.[10] Furthermore, antipyrine derivatives and their complexes with different metal ions can serve as antiparasitic agents and antitumor substances.[11,12] Moreover, azo dye metal complexes in which the azo group is included in bonding are derived from azo compounds comprising donor functions such as COOH, OH, SH, NH_2, in a congenial position so as to form five or six membered chelates.[13] In view of the obove facts and the importance of such azo dye bearing NO donor atoms,[12,13] we reported here the coordination character of azo dye ligand derived from 4-aminoantipyrine towards Mn (II), Co (II), Cr (III) and Cu (II) ions. The structural formulae of the complexes are investigated using analytical and spectral techniques. The molecular modeling was performed for the ligand and all complexes to assert their structural formula. Moreover, the antimicrobial efficiencies of the inspected compounds were examined towards different types of bacteria and fungi. Also, their antitumor activities were investigated against the human hepatocellular carcinoma cells HEPG2. Molecular docking analysis was achieved in silico to examine the ligand for its inhibitory performance on the receptor of 1zap (secreted aspartic protease from *Candida albicans*), 4ynt (*Aspergillus flavus* FAD glucose dehydrogenase), 3 t88 (*Escherichia coli*), and 4 m01 (*Staphylococcus aureus* adhesion protein). Different parameters like free energy of inhibition constant, Ki (μM), vdW + Hbond + desolv energy (kcal/mol), binding (kcal/mol), total intermolecular energy (kcal/mol), and electrostatic Energy (kcal/mol) and were determined. Also, the totally interaction profile (hydrogen bonds & hydrophobic interaction), and hydrogen bonding interactions (HB plot) were investigated.

2 | EXPERIMENTAL

1,3-Diphenyl-5-pyrazolone, anthranilic acid, triethylamine, ethanol, diethylether, DMSO, DMF, $MnCl_2 \cdot 4H_2O$, $CoCl_2 \cdot 6H_2O$, $CrCl_3 \cdot 6H_2O$ and $CuCl_2 \cdot 2H_2O$ were of high purity and was applied as purchased.

2.1 | Synthesis of azo Pyrazolone ligand (HL)

o-Amino benzoic acid (0.01 mol, 1.37 g) was dissolved in concentrated HCl (10 ml) and H_2O (10 ml), cooled to 5 °C and treated with a cold aqueous solution of $NaNO_2$ (0.01 mol, 0.69 g). The diazotized amine was added gradually to an ice-cold solution of 1,3-diphenyl-5-pyrazolone (0.01 mol, 2.25 g) in 10% aqueous NaOH (50 ml). After completing the addition process, the reaction mixture was left to stand in a cold chest for 12 hr. The obtained precipitate was filtered off, washed with H_2O and recrystallized using ethanol as an orange crystal of HL (Figure 1). The purity of ligand was examined applying melting point constancy and thin layer chromatographic (TLC) tools.

2.2 | Synthesis of the Nano-sized metal chelates

The following recommended general procedures were used. A hot ethanolic solution (30 ml) of HL (0.001 mol, 0.384 g) was mixed with 1 mM of the metals salts [$MnCl_2 \cdot 4H2O$ (0.1979 g), $CoCl_2 \cdot 6H_2O$ (0.2379 g), $CrCl_3Cl_2 \cdot 6H_2O$ (0.2664 g), $CuCl_2 \cdot 2H_2O$ (0.1705 g), dissolved in ethanol (40 ml) in the presence of six drops of triethylamine as a basic medium. The reaction mixture was mixed together and heated under reflux on water bath for 12 hours with occasional stirring. Both the presence of triethylamine as basic medium and contentious

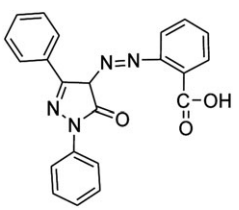

FIGURE 1 Molecular structure of 2-((5-oxo-1,3-diphenyl-4,5-dihydro-1H-pyrazol-4-yl)diazenyl) benzoic acid (HL)

stirring enhance the formation of nano-sized particles. The volume of the reaction mixture was reduced by evaporation of solvent until precipitation of the complex, which was filtered off and washed consequently with H_2O, warm ethanol and diethyl ether followed by drying in vacuum (over anhydrous calcium chloride).

2.3 | Instrumentations, measurements and methods

Perkin-Elmer 2400 CHN Elemental Analyzer was applied to determine C, H and N contents. The metal content was investigated by the aid of inductively coupled plasma (ICP) technique after decomposition of the metal complexes using nitric acid. The molar conductance of metal complexes were determined in DMF (10^{-3} mol L^{-1}) by the aid of a conductivity meter JENWAY model 4070 Conductance Bridge at room temperature. Infrared spectra were achieved as KBr discs using a Jasco FT-IR–4100 (Tsukuba, Japan) within 4000–200 cm^{-1} range. Standard electron impact mass spectra (E.I) of the free ligand and complexes 1–4 were performed by the aid of a Finnigan MAT 8222 Spectrometer at 70 eV. UV–Vis spectra were taken in freshly prepared DMF solution from 200 to 800 nm with T80 + UV–Vis spectrometer. Magnetic moments of the complexes were determined applying a Sherwood scientific magnetic susceptibility balance. EPR spectrum of Cu (II) complex (**4**) as powder was performed using a Jeol JES-RE1X EPR spectrometer working in the X-band, 9.435 GHz (at Alexandria University). XRD patterns of the inspected materials were obtained using a X-ray diffractometer (GNR, APD2000PRO, Italy) at Central Laboratory, Tanta University, Egypt. Whole patterns were measured at 0.03 ° min^{-1} scanning rate, applying Cu/Kα_1 radiation with a graphite monochromator. TGA (thermal gravimetric analysis) of complexes **1**–**4** were investigated (under nitrogen as atmosphere) using a Shimadzu TG-50 thermal analyzer from ambient temperature up to 800 °C (with 10 °C/min heating rate). Antifungal and antimicrobial activities of all compounds under interest were examined at Micro-Analytical Center, Cairo University applying a modified Kirby-Bauer disc diffusion method.[14,15] Evaluation of the antitumor activities of the investigated compounds against human liver *Carcinoma* cell lines (HEPG2) was carried out at the Regional Center for Microbiology and Biotechnology (Al-Azhar University) using the well-known recommended method.[15–17]

2.4 | Molecular docking using docking server

Docking Server software was applied to perform the molecular Docking calculations. The empirical charges were computed using MOPAC2009 and then added to the organic ligand atoms. Rotatable bonds were specified in the docking process, and non-polar hydrogen atoms were merged. The calculations were executed to validate the binding of the ligand with the receptor of 1zap (secreted aspartic protease from *Candida albicans*), 4ynt (*Aspergillus flavus* FAD glucose dehydrogenase), 3 t88 (*Escherichia coli*), and 4 m01 (*Staphylococcus aureus* adhesion protein). AutoDock tools were applied to append the solvation parameters, essential hydrogen atoms, and Kollman united atom type charges. In order to calculate the electrostatic terms, and the van der Waals, auto Dock parameter distance- and set- dependent dielectric functions were applied, respectively. The Solis & Wets local search method and The Lamarckian genetic algorithm (LGA) were applied in order to implement the docking simulations.

3 | RESULTS AND DISCUSSION

3.1 | Nature and stoichiometry of the formed complexes

The physical and analytical characteristics of the scrutinized ligand and complexes **1—4** are collected in Tables 1. The chemical composition and stoichiometry of the prepared metal complexes were confirmed by the results of elemental analysis. The gained data showed satisfactory coincidence within the proposed molecular formulae. These data supported formation of complexes exhibit 1:1 (M:L) stoichiometry. Complexes **1—4** were found to be stable in air (for a long time), insoluble in diversified organic solvents but soluble to great extent in DMSO and DMF. The molar conductance values (Table 1) are found to be within the range 8.50–14.00 Ω^{-1} cm^2 mol^{-1}. These values indicated the non-electrolytic character of the complexes **1—4**.[18] The metal complexes which contain chloride ion were also tested qualitatively with silver nitrate and no precipitation was detected which can be taken as a proof that the complexes are non-electrolytes.

3.2 | FT-IR and ^{1}H NMR spectra and bonding modes

The inspection of IR spectrum of the parent ligand HL compared with that of complexes **1—4 (Figure 1S)** denoted certain characteristics differences as presented in Table 2. The infrared spectra of the metal chelates were closely similar among themselves. In HL spectrum, the band appeared at 1520 cm^{-1} corresponding to $\nu_{N=N}$ shifted to higher frequency by 15–40 cm^{-1} in complexes **1—4** spectra supporting its coordination to Mn (II), Co (II), Cr (III) and Cu (II) ions.[19] The sharp carboxylic ν_{sym}

TABLE 1 Microanalysis, physical characteristics, and molar conductivity data of HL and complexes **1–4**

Comp. No.	Molecular formula (Empirical formulae)	M. Wt. Found (Calc.)	Colour (Λ_m)	Microanalysis; Found (Calc.) %			
				%C	%H	%N	%M
Ligand	HL ($C_{22}H_{16}N_4O_3$)	(384.55) (384.39)	Orange (---)	69.14 (68.74)	4.95 (4.20)	14.52 (14.58)	__ (---)
1	[MnLCl $(H_2O)_2$]•$2H_2O$ ($C_{22}H_{23}ClMnN_4O_7$)	(545.11) (545.83)	D. yellow (8.50)	48.36 (48.41)	4.36 (4.25)	10.49 (10.26)	9.98 (10.07)
2	[CoLCl (H_2O)]•C_2H_5OH ($C_{24}H_{23}ClCoN_4O_5$)	(541.11) (541.85)	D. brown (10.00)	52.97 (53.20)	4.76 (4.28)	10.52 (10.34)	10.00 (10.88)
3	[$CrLCl_2(H_2O)$]•$2H_2O$ ($C_{22}H_{21}Cl_2CrN_4O_6$)	(560.01) (560.33)	D. Orange (14.00)	46.78 (47.16)	5.88 (3.78)	9.55 (10.00)	9.74 (9.28)
4	[CuLCl]•H_2O ($C_{22}H_{17}ClCuN_4O_4$)	(500.74) (500.39)	Green (11.00)	52.49 (52.81)	3.12 (3.42)	11.30 (11.20)	12.55 (12.70)

TABLE 2 Important IR spectral bands (cm^{-1}) and their assignment for the ligand **HL** and its metal complexes

Compounds	IR spectra					
	$N_{N=N}$	$\nu_{C=O}$ (ring)	$\nu_{C=N}$ (ring)	$\nu_{sym(COO-)}$	ν_{M-O}	ν_{M-N}
HL	1520	1665	1493	1783	--	--
1	1560	1656	1487	1734	603	504
2	1556	1658	1489	1712	612	433
3	1553	1652	1489	1727	609	491
4	1535	1647	1497	1727	612	492

(COO^-) of the free ligand HL appeared at 1783 cm^{-1} showed obvious shifts to lower frequencies in the metal complexes, and appeared within 1712–1734 cm^{-1} range. This behavior confirmed that the ligand coordinates to the metal ions through the O-atom of the carboxylate group. The stretching band of carbonyl group ν (C=O) of 5-pyrazolone moiety did not show significant wavenumber shift in complex **2** indicating non-participation of the carbonyl-O atom in binding to Co (II), whereas; appreciable downward wavenumber shifts 9–18 cm^{-1} in complexes **1**, **3**, and **4** confirming that oxygen atom of pyrazolone moiety was coordinated to Mn (II), Cr (III) and Cu (II) ions. According to these IR data, HL behaves as monobasic tri-dentate ligand towards Mn (II), Ni (II) and Cu (II) and monobasic bi-dentate towards Co (II). In the spectra complexes **1—4**, the broad band around 3429–3440 cm^{-1} are attributed to the presence of coordinated water. Appearance of non-ligand bands ranging between 603–612 cm^{-1} and 433–504 cm^{-1} in the complexes are characteristic of M-O and M-N bands, respectively.[15]

The ^1H NMR spectrum of the investigated ligand **HL** (Figure 2S) showed two singlets at 14.91 and 12.06 ppm; each one is integrated for one proton. NH Proton of the pyrazolone ring appeared in the same position as **HL** which elucidates the assignment of NH proton of the pyrazolone ring. The proton at 4 position of the pyrazolone ring appears as a singlet at 7.67 ppm inside the multiplet region. The multiplet at 7.26–8.11 ppm is due to the aryl protons of the two benzene rings.

3.3 | Inspection of mass spectra

Mass spectra were applied to underline the constitutions and pureness of the synthesized ligand and its chelates (Figure 3S). The free ligand fragmentation showed the molecular ion peak at 384.55, which is coincide with its theoretical value (384.39). Mass spectra of [MnLCl $(H_2O)_2$]•$2H_2O$, [CoLCl (H_2O)]•C_2H_5OH, [$CrLCl_2(H_2O)$]•$2H_2O$, [CuLCl]•H_2O presented precise molecular ion peaks (calc.) at 545.11 (545.83), 541.11 (541.85), 560.01 (560.33), 500.74 (500.39), respectively, corresponding to the parent ion $[ML]^+$. Also, appearance of various peaks due to assorted fragments trough sequential degradation of the base compound is excellent evidence supporting the proposed molecular structure [15]. Ideal evidence backing the suggested structures of the complexes result from the decomposition of complexes **1—4** *via* elimination of HL, which confer rise to the occurrence of a molecular ion peak assignable to the free ligand. This is triumphant

character for metal complexes involving various types of ligands (ML) that decompose *via* incision of the ligand–metal bond during the ionization process.[20]

3.4 | Thermo-gravimetric analytical studies

The TGA curves of complexes **1—4** were on performed under N_2 gas flow from ambient temperature up to 800 °C at a heating rate of 10 °C/min (Figures 4S). Applying TGA curves, the mass loss was determined for the various thermal degradation stages in comparison with those theoretically computed for the suggested formula depending on the results of micro-analyses. In generality, TGA denoted the formation of metal oxide as a residue from which the percentage of metal (%) is calculated and found to be in favorable conformity with that gained from analytical measurements.[21] The acquired data showed that complexes **1—4** decomposed in four steps for complex **1** and three steps for complexes **2**, **3** and **4**. The decomposition steps, theoretical calculated, and found mass losses, temperature ranges, as well as final products observed in each thermal decomposition process are presented in Table 3.

3.5 | Thermo-kinetic parameters

The order of reaction (n) mechanism of thermal degradation process, frequency factor (*A*), andactivation energy (*E*), for various stages in thermal decomposition complexes **1—4** were investigated using integral method suggested by Coats-Redfern (Figures 5S-8S).[22] The thermo-kinetic activation parameters of thermal decomposition steps of complexes **1—4** are presented in Tables 1S and prove the following points;

a- ΔH^* exhibited positive values denoting the endothermic nature of all thermal decomposition processes.
b- ΔS^* have positive values for complexes **1—4**, revealing that the activated complex is less ordered compared with the reactants and/or the reactions are very quick.[23]
c- Increasing of ΔG^* values in appropriately or significant way for the subsequently decomposition steps as a result of increasing $T\Delta S^*$ values on going from one step to another which disregard values of ΔH^*. This reverberates that the rate of abstraction of the posterior parts of ligand will be lower than that of the forerunner.[24] This can be bemoaned to the structural rigidity of the vestige complex after libration of one or more ligand parts, in comparison with the precedent complex, which needs more energy for its rearrangement before sustaining any further compositional alteration.

3.6 | ESR Spectrum of cu (II) complex

The powder X-band ESR spectra of Cu (II) complex (**4)** at room temperature displayed a broadened characteristic without hyperfine splitting due to the dipolar interaction from the ESR spectrum of a set of magnetic parameters.

TABLE 3 Thermogravimetric analysis (TGA) of complexes **1—4**

No	Molecular formula (Empirical formulae)	Temp. range (°C)	Mass loss %		Assignment
			Found	Calc.	
1	$[MnLCl(H_2O)_2]\cdot 2H_2O$ ($C_{22}H_{23}ClMnN_4O_7$)	31–93	6.68	6.59	Loss of hydrated $2H_2O$ molecules.
		93–225	6.79	6.59	Removal of coordinated $2H_2O$ molecules.
		225–346	28.03	28.48	Elimination of Cl, CO_2, C_6H_5.
		346–390	45.50	45.31	Decomposition of the organic ligand and formation of MnO as a residual product.
2	$[CoLCl(H_2O)]\cdot C_2H_5OH$ ($C_{24}H_{23}ClCoN_4O_5$)	31–85	8.50	8.48	Evaporation of C_2H_5OH molecule.
		85–326	29.50	29.62	Removal of H_2O, Cl, CO_2, C_5H_3.
		326–376	46.00	45.83	Decomposition of the organic ligand and formation of CoO + C as a final product.
3	$[CrLCl_2(H_2O)]\cdot 2H_2O$ ($C_{22}H_{21}Cl_2CrN_4O_6$)	45–115	7.22	6.42	Removal of hydrated $2H_2O$ molecule.
		115–287	16.23	15.88	Loss of coordinated H_2O + 2Cl molecules.
		287–470	54.29	55.53	Decomposition of the organic ligand and formation of Cr + 6C as final product.
4	$[CuLCl]\cdot H_2O$ ($C_{22}H_{17}ClCuN_4O_4$)	40–140	3.40	3.59	Loss of hydrated H_2O molecule.
		140–301	6.22	7.09	Loss of coordinated Cl molecules.
		301–465	71.46	71.02	Decomposition of the organic ligand and formation of CuO + C as a residue.

Two anisotropic signals was appeared in ESR spectrum of Cu (II) complex **4** (Figure 9S). The shape of ESR spectrum supports tetrahedral geometry around Cu (II) center. Cu (II) complex **4** showed g_{eff}-value (2.1222) with a positive mutation from the free electron value (2.0023) which is assigned to the significant covalent character in the bonding between the ligand and Cu (II) ion. Hence, the metal ligand bonding in these complexes exhibit ultimately covalent character.[25]

3.7 | UV–vis spectra and magnetic moment studies

The electronic absorption spectra of ligand and complexes **1—4** were achieved applying in Nujol mull technique. The spectrum of HL displayed band at 24752 cm^{-1} corresponding to charge transfer transition within the ligand molecule. This band exhibited red shift in the range 422–1168 cm^{-1} in complexes **1—4** spectra supporting the participation of C=O and N=N in complex formation.[26] The calculated magnetic moment value for Mn (II) complex 1 was found to be 6.10 B.M. The spectrum of the Mn (II) complex displayed a weak bands at 17391 and 23255 cm^{-1} corresponding to the $^6A_1g \rightarrow {}^4Eg(4D)$ and $^6A_1g \rightarrow {}^4T_1g(4D)$ transitions, respectively.[27] These results supported the high spin octahedral geometry around the Mn (II) ion and considerable covalent character.[28] Co (II) complex **2** presented two bands at 17513 and 28326 cm^{-1} which can be attributed to $^4A_2 \rightarrow {}^4T_1(F)$, $^4A_2 \rightarrow {}^4T_1(P)$ transitions, respectively, in a tetrahedral arrangement.[29] Complex **2** exhibited a moment value equals 3.80 BM confirming its paramagnetic character. Cr (III) complex 3 showed two bands at 18726, and 27322 cm^{-1} can be assigned to $^4B_{1g} \rightarrow {}^4E^a_g$, and $^4B_{1g} \rightarrow {}^4E^b_g$ transitions, respectively, reinforcing the lifting of the degeneracy of the orbital triplet (in octahedral symmetry) in the order of increasing energy and assuming D_{4h} symmetry.[30] It has 5.40 BM magnetic moment values in agreement with the suggested geometry. Cu (II) complex **4** showed a band at 18552 cm^{-1} attributed to $^2T_2 \rightarrow {}^2E$ transition supporting tetrahedral geometry around the central Cu (II) ion. The subnormal μ_{eff} value of Cu (II) complex (1.10 BM) announces the Cu-Cu interaction.[31]

3.8 | XRD studies

Meaningful structural data concerning microcrystalline nature of HL and complexes **1—4** can be obtained from inspecting their XRD.[32] The diffraction pattern of all compounds were achieved within 2θ (scattering angle) from 10 to 90°. XRD pattern of free ligand HL are fully different compared with those of each metal complex (Figure 2), supporting complex formation. The XRD

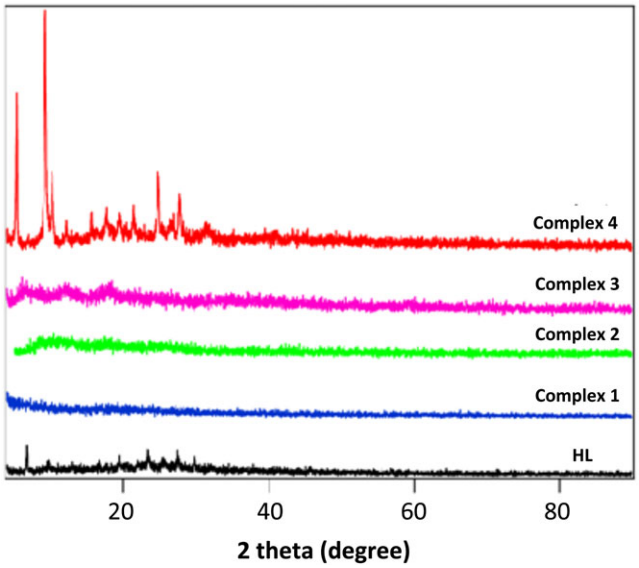

FIGURE 2 XRD spectral patterns of HL and complexes **1—4**

patterns revealed that Cu (II) complex **4** exhibit nanocrystalline phase, whereas HL and complexes **1—4** showed amorphous nature. This behavior may supposedly be assigned to the incorporation of the H_2O molecules. A comparative analysis between the patterns of ligand and those of metal complexes refers to the absence of smearing or contamination with starting reactants. The value of average particle size of Cu (II) complex **4** was calculated applying the Deby-Scherrer equation, and found to be 5.3627 nm.

The occurrence of the novel compounds in such scrupulous modernistic nanometer scale ordinarily attract formidable attention due to their outstanding functional properties and a wide range of interesting technological applications, including microelectronics, optics, catalysis, chemical and bio-sensors.[33]

3.9 | Molecular modeling studies

The model geometric structures of HL and complexes **1—4** have been achieved by optimization of their bond lengths, dihedral angles and bond angles, using the hyper chem. 8.03 molecular modeling program.[34] The structures were optimized (Figures 3–7) with minimum energies acquired applying the quantum chemical calculations. Selected bond lengths and bond angles of significant importance are presented in Tables 2S–6S. As shown presented in Figure 3, the studied ligand has a planner form. The bond lengths between atoms in coordination center are C(3)-O(13) = 1.192, C(4)-N(14) = 1.318, N(14)-N(15) = 1.338, N(15)-C(21) = 1.452, C(27)-O(28) = 1.366 and C(27)-O(29) = 1.208 Å. Upon chelation, the bond lengths of free ligand HL are altered to some extent, essentially for the atoms in direct interaction

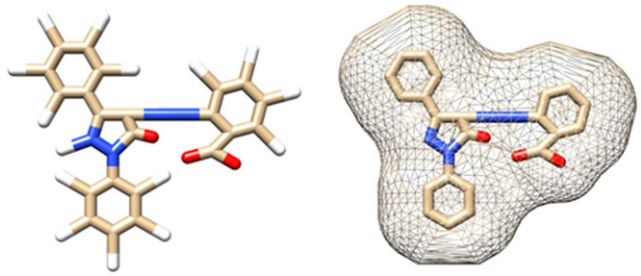

FIGURE 3 Optimized molecular structure of 2-((5-oxo-1,3-diphenyl-4,5-dihydro-1H-pyrazol-4- yl)diazenyl) benzoic acid (HL)

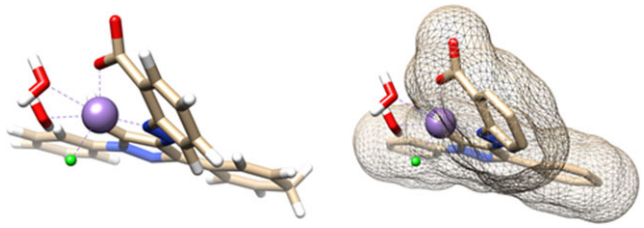

FIGURE 4 Optimized molecular structure of Mn (II)-complex (**1**)

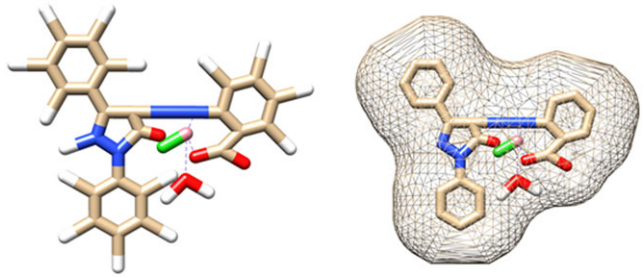

FIGURE 5 Optimized molecular structure of Co (II)-complex (**2**)

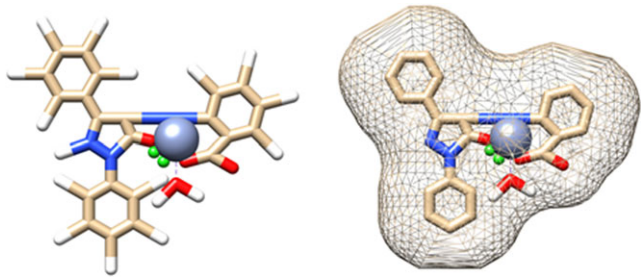

FIGURE 6 Optimized molecular structure of Cr (III)-complex (**3**)

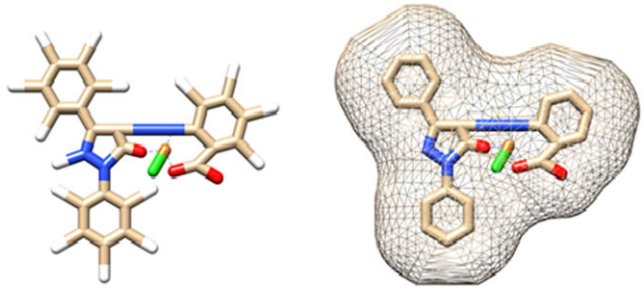

FIGURE 7 Optimized molecular structure of Cu (II)-complex (**4**)

with the metal ions. Otherwise, the bond lengths of the rest atoms in HL are slightly or not altered upon chelation with the metal ions under interest. The optimization revealed that Mn (II) complex **1** has an octahedral geometry. The bond lengths of central metal atom with the chelating atom are Mn(31)-N(20) = 1.786, O(29)-Mn(31) = 1.888, O(22)-Mn(31) = 1.884, Mn(31)-O(35) = 2.375 and Mn(31)-O(32) = 1.893 Å. Also, The bond lengths of Cr (II) ion with the chelating atoms are Cr(30)-N(15) = 1.968, O(13)-Cr(30) = 1.937, O(29)-Cr(30) = 1.847, Cr(30)-Cl(31) = 2.260, Cr(30)-O(33) = 1.968 Å. The bond angles around Mn and Cr atoms (Tables 3S and 5S) are quite near to an octahedral geometry,[35] indicting sp^3d^2 hybridization. Co (II) and Cu (II) complexes are found to attain distorted tetrahedral structures where the hydroxyl oxygen atom and N-atom are coordinated to the metal center. In Cu (II) complex **4**, the bond lengths of Cu atom and chelating atoms are Cu(30)-N(15) = 1.902, O(13)-Cu(30) = 1.849, O(29)-Cu(30) = and Cu(30)-Cl(31) = 2.160 Å. The bond angles of ligand are changed upon chelation with Cu (II) and Co (II) ions. The largest changes occur for those bonding the N-atom and hydroxyl oxygen supporting their co-ordination to the metal centers (Tables 4S and 6S). As example, the optimization bond angles around Co-atom are C(31)-N(15)-Co(30) = 115.66, N(15)-Co(30)-Cl(31) = 110.79, Co(30)-O(32)-H(33) = 109.47 and O(29) Co(30)-O(32) = 110.80, which confirms the distorted tetrahedral geometry of the complex **2**. The computed bond angles around Cu atom are C(3)-O(13)-Cu(30) = 116.02, O(13)-Cu(30)-N(15) = 100.12, N(15)-Cu(30)-O(29) = 97.38 and C(21)-N(15)-Cu(30) = 125.17°. From the change between minimum and maximum bond angles around Co (II) and Cu (II) ions distorted tetrahedral geometries are proposed.[36] The evanescence of O-H bond and appearance of novel M-O bond supported the participation of carboxylic hydroxyl group in chelate formation.[37] As a result of electronegativity difference between the oxygen and nitrogen atoms, the M-O bond length differs than that of M-O bond.[38,39]

3.10 | In-vitro antifungal and antibacterial assays

The in-vitro antimicrobial efficiencies of HL and the inspected complexes **1—4** were examined against *E. coli, P. vulgaris, S. aureus, B. subtillis, A. fumigatus* and *C. albicans* stratify the modified Kirby–Bauer disc diffusion technique.[14,15] The obtained results are displayed in Table 7S. The free ligand under interest and complexes **1—4** did not display any anti-fungal activities against the examined organisms. The free organic ligand and complexes **1—4** showed moderate to high efficiencies across

E. coli and *P. vulgaris*. Furthermore, the HL and complexes **2** and **3** exhibited moderate activities against *S. aureus* and *B. subtillis*. This character may be clearfield depending on the concepts of chelation theory.[40] This theory states that a diminution in the metal polarizability could reinforce the lipophilicity of the metal complexes. This causes a slump of the permeability of the cells, resulting in intervention with normal processes of the cells. Hence, the complexation leads to make the azo compounds act as more potent and vigorous antimicrobial agents, inhibiting the growth of bacteria more and more compared with than the parent organic ligand.[41] So, it is concluded that the chelation process significantly affects the efficacy of materials that are potent towards microbial strains.

3.11 | Antitumor activity evaluation

Novel anticancer agents are in need to combat the acquired drug resistance often seen in cancer patients.[42] The anticancer performance of HL and complexes **1—4** was detected *in vitro* against human hepatocellular carcinoma cells (HEPG2) utilizing Doxorubicin (Dox) as a reference drug (IC_{50} = 4.73). Also, the untreated cells were applied as a reference control. Each data point was determined as the average of three separated experiments and specified as mean ± SD. Growth inhibition of 50% (IC_{50}) is determined as the compound concentrations, which leads to a 50% lowering in cell proliferation pending the tested compound incubation.[43] From the gained results it is shown that the growth inhibition of the tested cells is strongly affected by the character of metal ion and increases in the order; Mn (II) complex < Cr (III) complex < Co (II) complex < Cu (II) complex < HL. This denotes that the type of metal ion play a significant role in determining the anticancer efficiency.[44] According to Shier.[45] the compounds displaying IC_{50} values within 10.00–25.00 μg/ml range are considered weak anticancer agents, compounds exhibit IC_{50} value between 5.00–10.00 μg/ml are moderate, whereas those below 5.00 μg/ml are strong anticancer agents. HL and complexes **1, 2, 3** and **4** exhibited a weak activity towards human liver *Carcinoma* cell line (HEPG2) and showed IC_{50} values of 15.3, 174, 52.4, 102 and 23.5 μg/ml, respectively.

3.12 | Molecular docking analysis

The inhibition constant, Ki (μM), free energy of binding, total estimated energy of vdW + Hbond + desolv (kcal/mol), total intermolecular energy parameters and electrostatic energy were computed to evaluate the favorable binding of HL to the proteins. Table 4 presented the complete profile of all mentioned parameters of HL for its interaction with receptor of 4 m01 (*Staphylococcus aureus* adhesion protein), 3 t88 (*Escherichia coli*), 1zap (secreted aspartic protease from Candida albicans), and 4ynt (*Aspergillus flavus* FAD glucose dehydrogenase). One of the most favorable bindings of the ligand was its binding with 4ynt and 3 t88 and proteins with evaluated free energy of binding −6.91 and − 6.98 kcal/mol, respectively. Also, the ligand showed the inhibition constant (ki) of 7.59 and 8.56 μM of 3 t88 and 4ynt, respectively. Figure 10S displays the binding of the azo pyrazolone ligand (HL) to the protein 3 t88. A 2D plot was generated where hydrogen bonds, non-ligand bond, and ligand bond, in addition to their lengths were mentioned (Figure 10S). A HB plot has been generated to mention interactions with various amino acids of the protein (Figure 8). Similarly, Figures 11S–16S showed the binding pattern of the azo pyrazolone ligand (HL) with 1zap (secreted aspartic protease from *Candida albicans*), 4ynt

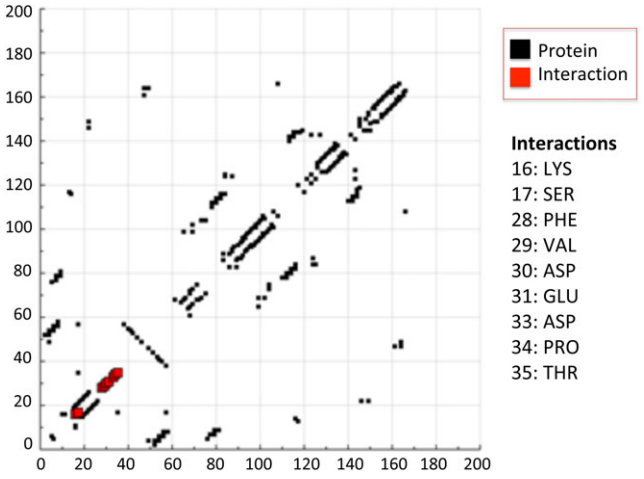

FIGURE 8 HB plot of interaction between azo pyrazolone ligand (HL) and receptor of *Escherichia coli* (3 t88)

TABLE 4 Binding energies for the interactions between azo pyrazolone ligand (HL) and 3t88, 4m01, 1zap and 4ynt

Interaction	Est. Free Energy of Binding (kcal/mol)	Est. Inhibition Constant, Ki (μM)	vdW + Hbond + desolv Energy (kcal/mol)	Electrostatic Energy (kcal/mol)	Total Intermolec. Energy (kcal/mol)
Ligand-3 t88	−6.98	7.59	−8.94	−0.02	−8.96
Ligand-4 m01	−4.64	394.25	−5.53	+0.06	−5.47
Ligand-1zap	−5.87	49.61	−7.63	−0.04	−7.67
Ligand-4ynt	−6.91	8.56	−8.07	−0.01	−8.08

(*Aspergillus flavus* FAD glucose dehydrogenase), and 4 m01 (*Staphylococcus aureus* adhesion protein). Colletively, the in silico molecular docking analysis confirm the in vitro findings of the anti-microbial activity of azo pyrazolone ligand (HL) and possibly its complexes. Hence, our findings present these complexes as novel nano-synthesized azopyrazolone complexes with antimicrobial activities.

4 | CONCLUSION

Four novel nano-size Mn (II), Co (II), Cr (III) and Cu (II)] complexes with 2-((5-oxo-1,3-diphenyl-4,5-dihydro-1H-pyrazol-4-yl)diazenyl) benzoic acid (HL) were synthesized. The complexes were investigated using spectral (FT-IR, UV–Vis, ESR, MS), thermal and elemental analyses. The XRD confirmed the nano-sized nature of Cu (II) complex. Mn (II) and Cr (III) complexes have octahedral arrangement while Co (II) and Cu (II) complexes have distorted tetrahedral configuration. Molecular modeling was performed by the molecular mechanic calculation using the hyper chem. 8.03 molecular modeling program to give the most stable geometry. The mechanism, E, n, ΔH^*, ΔS^*, A, and G* values for thermal decomposition of the inspected complexes were determined from TGA curves applying Coats-Redfern method. Azo pyrazolone ligand (HL) and complexes **1—4** displayed a weak anticancer activity and a reasonable anti-microbial activity as confirmed by the in vitro and in silico studies.

ORCID

Mohamed Gaber http://orcid.org/0000-0003-2315-5710
Abdalla M. Khedr http://orcid.org/0000-0002-4119-5401

REFERENCES

[1] J. I. Saad, A. El Achari, *J. Mol. Struct.* **2018**, *1154*, 557.

[2] M. A. Abdelgawad, M. B. Labib, W. A. M. Ali, G. Kamel, A. A. Azouz, E. EL-Nahass, *Bioorg. Chem.* **2018**, *78*, 103.

[3] G. Mariappan, B. Saha, L. Sutharson, A. Singh, S. Garg, L. Pandey, D. Kumar, *Saudi Pharm. J.* **2011**, *19*, 115.

[4] N. Parekh, K. Maheria, P. Patel, M. Rathod, *Int. J. Pharm. Tech. Res.* **2011**, *3*, 540.

[5] S. R. Kamat, R. S. Salunkhe, P. B. Choudhari, R. P. Dhavale, A. H. Mane, T. R. Lohar, *Res. Chem. Intermed.* **2018**, *44*, 1351.

[6] P. Manojkumar, T. Ravi, G. Subbuchettiar, *Acta Pharm.* **2009**, *59*, 159.

[7] A. Zaoui, Hammal, N. Bennamane, S. Merabtene, B. N. Kolli, *Int. J. Pharm. Bio. Sci.* **2013**, *3*, 732.

[8] S. E. Forest, M. J. Stimson, J. D. Simon, *J. Phys. Chem. B* **1999**, *103*, 3963.

[9] P. Santos, A. Antunes, J. Noronha, E. Fernandes, A. J. S. C. Vieira, *Eur. J. Med. Chem.* **2010**, *45*, 2258.

[10] A. A. S. Al-Hamdani, W. Al-Zoubi, *Spectrochim. Acta A* **2015**, *137*, 75.

[11] T. Aysha, A. Lycka, S. Lunák Jr., O. Machalický, M. Elsedik, R. Hrdina, *Dyes Pigm.* **2013**, *98*, 547.

[12] M. N. Al-Jibouri, *Eur. Chem. Bull.* **2014**, *3*, 447.

[13] R. Gup, B. Kirkan, *Spectrochim. Acta A* **2005**, *62*, 1188.

[14] A. C. Scott, Laboratory Control of Antimicrobial therapy, in *Practical Medical Microbiology*, 13th ed. (Eds: J. G. Collee, J. P. Duguid, A. G. Frasa, B. D. Marmion), Churchill Livingestone, Edinburgh 1981.

[15] M. Gaber, A. M. Khedr, M. Elsharkawy, *Appl. Organomet. Chem.* **2017**, *31*. https://doi.org/10.1002/aoc.3885

[16] T. Mosmann, *J. Immunol. Methods* **1983**, *65*, 55.

[17] A. P. Wilson, in *Cytotoxicity and viability assays in animal cell culture: A practical Approach*, 3rd ed. (Ed: J. R. W. Masters), Oxford University Press, Oxford **2000**.

[18] D. C. Onwudiwe, A. C. Ekennia, E. Hosten, *J. Coord. Chem.* **2016**, *69*, 2454.

[19] A. M. Khedr, M. Gaber, K. M. Saad-allah, *Chin. J. Inorg. Chem.* **2014**, *30*, 1201.

[20] B. K. Singh, P. Mishra, B. S. Garg, *Transition Met. Chem.* **2007**, *32*, 603.

[21] K. Y. El-Baradie, M. Gaber, *Chem. Pap.* **2003**, *57*, 317.

[22] J. Liu, D. Song, H. Guan, *Russ. J. Appl. Chem.* **2016**, *89*, 1009.

[23] C. R. Vinodkumar, M. K. Muraleedharan, P. K. Radhakrishnan, *J. Therm. Anal. Calorim.* **2000**, *61*, 143.

[24] W. H. Mahmoud, G. G. Mohamed, M. M. I. El-Dessouky, *Spectrochim. Acta A* **2014**, *122*, 598.

[25] T. M. A. Ismail, *J. Coord. Chem.* **2005**, *58*, 141.

[26] A. Z. El-Sonbati, M. A. Diab, A. A. El-Bindary, S. G. Nozha, *Spectrochim. Acta A* **2011**, *83*, 490.

[27] S. Chandra, L. K. Gupta, *Ind. J. Chem. Soc.* **2005**, *82*, 454.

[28] K. Siddappa, M. Kote, P. C. Reddy, T. Reddy, *J. Chem. Pharm. Res.* **2011**, *3*, 780.

[29] N. El-wakiel, M. El-keiy, M. Gaber, *Spectrochim. Acta A* **2015**, *147*, 117.

[30] A. M. A. Alaghaz, R. A. Ammar, *Eur. J. Med. Chem.* **2010**, *45*, 1314.

[31] M. Gaber, N. A. El-Wakiel, H. El-Ghamry, S. K. Fathalla, *J. Mol. Struct.* **2014**, *1076*, 251.

[32] A. A. Fahem, *Spectrochim. Acta A* **2012**, *88*, 10.

[33] A. Salimi, R. Hallaj, S. Soltanian, *Biophys. Chem.* **2007**, *130*, 122.

[34] *HyperChem Version 8.03*, Hypercube, Inc., Gainesville, FL.

[35] K. El-Baradie, N. A. El-Wakiel, H. A. El-Ghamry, *Appl. Organomet. Chem.* **2015**, *29*, 117.

[36] S. Amer, N. A. El-Wakiel, H. A. El-Ghamry, *J. Mol. Struct.* **2013**, *1049*, 326.

[37] A. Despaigne, J. Silvva, A. Carmo, O. Piro, E. Castellano, H. Beraldo, *J. Mol. Struct.* **2009**, *920*, 97.

[38] T. A. Yousef, G. M. Abu El-Reash, R. M. El Morshedy, *J. Mol. Struct.* **2013**, *1045*, 145.

[39] T. A. Yousef, G. M. Abu El-Reash, R. M. El-Morshedy, *Polyhedron* **2012**, *45*, 71.

[40] A. M. Khedr, M. Gaber, E. H. Abd El-Zaher, *Chinese J. Chem.* **2011**, *29*, 1124.

[41] A. Kulkarni, P. G. Avaji, G. B. Bagihalli, S. A. Patil, P. S. Badami, *J. Coord. Chem.* **2009**, *62*, 481.

[42] A. S. Sultan, H. Brim, Z. A. Sherif, *Cancer Sci.* **2008**, *2*, 272.

[43] S. H. Etaiw, S. A. Amer, M. M. El-Bendary, *J. Inorg. Organomet. Polym.* **2011**, *21*, 662.

[44] X. Riera, V. Moreno, C. J. Ciudad, V. Noe, M. Font-Bardía, X. Solans, *Bioinorg. Chem. Appl.* **2007**, 98732.

[45] W. T. Shier, *Mammalian Cell Culture on $5 a Day: A Lab Manual of Low Cost Methods*, University of the Philippines, Los Banos **1991**.

SUPPORTING INFORMATION

Additional supporting information may be found online in the Supporting Information section at the end of the article.

How to cite this article: Gaber M, Khedr AM, Mansour MA, Elsharkawy M. Nano-synthesis, characterization, modeling and molecular docking analysis of Mn (II), Co (II), Cr (III) and Cu (II) complexes with azo pyrazolone ligand as new favorable antimicrobial and antitumor agents. *Appl Organometal Chem*. 2018;32:e4606. https://doi.org/10.1002/aoc.4606